Carbon Trends 25 (2026) 100716

Contents lists available at ScienceDirect

Carbon Trends

journal homepage: www.elsevier.com/locate/cartre

Efficient removal of polymer residues from graphene by sequential solvent cleaning

Monika Choudhary [a,*], Rasuole Lukose [a], Moriom Akter [a], Christian Wenger [a,b], Mindaugas Lukosius [a]

[a] IHP—Leibniz-Institute for High-Performance Microelectronics, Frankfurt Oder, Germany
[b] Semiconductor Materials, BTU Cottbus-Senftenberg, Cottbus, Germany

ARTICLE INFO

Keywords:
Graphene
PMMA
Transfer
Solvent
Carbon
Cleaning

ABSTRACT

Despite advances in graphene's synthesis, integrating graphene into functional devices requires its transfer from growth substrate onto electrically insulating target substrates, such as SiO_2/Si, a step that must preserve the structural and electronic integrity of graphene. However, residual poly (methyl methacrylate) (PMMA) after transfer severely impacts graphene's intrinsic properties. To address this, we introduced an improved post transfer cleaning method using a commercial PMMA remover in combination with acetone, applied at varying durations (3–10 min) and sequences. A remover-first sequence at 5 min was found to be most efficient in residue removal, as identified by an atomic force microscopy (AFM) root-mean-square (RMS) roughness of $\sim 0.54\ nm$ (comparable to bare SiO_2/Si) and a micro-Raman 2D-band full width at half maximum (FWHM) of $31.29 \pm 0.19\ cm^{-1}$, close to as-grown values. This improvement was rationalized using Hansen solubility parameters, which describe the differential affinity of each solvent for PMMA versus adventitious surface contaminants.

1. Introduction

Realizing graphene's industrial potential requires reproducible, wafer-scale synthesis on CMOS-compatible substrates. Among current growth approaches, chemical vapor deposition (CVD) of monolayer graphene on epitaxial Ge/Si as growth substrates, has emerged as one of the most promising methods [1–5]. However, integrating graphene into functional devices, necessitates a defect-free transfer of graphene onto patterned insulating substrates, such as SiO_2/Si. Among the transfer methodologies reported including roll-to-roll, bubble, and sacrificial layer-assisted transfer, poly (methyl methacrylate) (PMMA)-assisted wet transfer remains the most widely adopted technique for CVD grown graphene, owing to its procedural simplicity, and compatibility with wafer-scale films [6–11]. This approach, however, introduces several significant challenges. The mechanical stresses exerted during film delamination and handling frequently result in tears, cracks, folds, and local delamination of the graphene layer. More critically, complete removal of the PMMA after the transfer has proven extremely difficult. Residual PMMA fragments and nanoscale polymer clusters invariably persist on the graphene surface after solvent treatment. These surface adsorbates act as charge impurity scattering centers, induce unintentional doping, and locally perturb the electronic band structure, collectively degrading carrier mobility, and device reproducibility [7,8,12–14]. Considerable effort has therefore been devoted to developing effective post-transfer cleaning strategies that can remove polymer residues without introducing additional damage or contamination to the graphene lattice. The principal approaches include thermal annealing [15–17], current-induced Joule heating, AFM-based mechanical cleaning [18–20], plasma treatment [21,22], and chemical solvent cleaning, each carrying distinct advantages and limitations [22].

Among all post-transfer cleaning strategies, chemical solvent cleaning remains the most practically accessible approach in integrated graphene technology [23]. Acetone and chloroform are the most commonly used solvents due to their ability to dissolve bulk PMMA; however, both solvents leave behind a nanometer-thick layer of polymer residues strongly adsorbed on the graphene surface, which resists complete removal by further solvent rinsing alone [22,24]. Stronger polar aprotic solvents such as N-methyl-2-pyrrolidone (NMP) offer improved

* Correspondence author.
E-mail addresses: choudhary@ihp-microelectronics.com (M. Choudhary), lukose@ihp-microelectronics.com (R. Lukose), akter@ihp-microelectronics.com (M. Akter), wenger@ihp-microelectronics.com (C. Wenger), lukosius@ihp-microelectronics.com (M. Lukosius).

https://doi.org/10.1016/j.cartre.2026.100716
Received 9 September 2026; Received in revised form 26 October 2026; Accepted 7 November 2026
Available online 7 November 2026
2667-0569/© 2026 The Authors. Published by Elsevier Ltd. This is an open access article under the CC BY license (http://creativecommons.org/licenses/by/4.0/).
Open access funding enabled and organized by Projekt DEAL.

solvation of adsorbed polymer chains due to their higher solubility parameter and stronger dipole–dipole interactions with PMMA; however, has been reported that prolonged NMP treatment introduce lattice defects, promote graphene delamination from weakly adhering substrates, and leave NMP-specific residues that are themselves difficult to remove [23]. More recently, the commercial remover AR 600–71, used in combination with acetone, has demonstrated improved cleaning performance comparative to acetone treatment alone, reducing the RMS surface roughness from 2.2 *nm* to 0.7 *nm* and yielding hole and electron field-effect mobilities as high as 9000 and 8000 $cm^2V^{-1}s^{-1}$ [23]. To date, the physicochemical mechanisms underlying the enhanced cleaning performance of this remover in relation to acetone, has not been reported in the literature. Critical parameters governing residue removal efficiency, including the thermodynamic compatibility between the solvent components and the adsorbed PMMA phase, the optimal treatment duration and the influence of solvent application sequence on the final residual PMMA have not been investigated. Furthermore, it is important to note that the vast majority of published studies on graphene transfer and post-transfer cleaning pertain to graphene grown on metallic foil substrates, particularly copper, which exhibit substantially different surface chemistry, graphene–substrate interaction strength, and residue characteristics compared to graphene grown on semiconductor Ge/Si substrates. The specific transfer and cleaning behavior of CVD graphene grown on Ge/Si, which is of direct relevance to CMOS-compatible device integration, remains largely unexplored and poorly understood.

In this work, we present a systematic study of wafer-scale monolayer graphene grown by CVD on Ge/Si substrates transfer onto SiO_2/Si target substrates using electrochemical delamination-assisted PMMA wet transfer. We investigate the effect of treatment time, varied from 3 to 10 min in both AR 600–71 remover and acetone on the efficiency of PMMA residue removal, as characterized by AFM, XPS, and Raman spectroscopy. In addition, the sequential order of remover and acetone treatment is reversed to assess the influence of treatment sequence on the final surface cleanliness. Hansen solubility parameter analysis is employed as a thermodynamic framework to rationalize the observed dependence of residue removal efficiency on solvent type, treatment duration, and sequence, providing mechanistic insight into the polymer dissolution behavior at the graphene surface. We observed that remover first sequence at time T2 (5 min) yielded cleanest graphene films with RMS roughness of 0.54 *nm* approaching intrinsic SiO_2/Si roughness values (0.49 *nm*).

2. Methods and experiments

2.1. Growth

Monolayer graphene was synthesized on epitaxial Ge(110) layers by CVD using a Black Magic BM300T cold-wall reactor (Aixtron, Germany). Prior to graphene growth, 2 μm thick epitaxial Ge films were deposited on 200 mm Si(110) wafers via CVD to provide a well-defined crystalline growth template. Monolayer graphene was subsequently grown at deposition temperature of 885 °C and a chamber pressure of 700 mbar from a CH_4/H_2 precursor mixture with Argon serving as the carrier gas.

2.2. Graphene transfer

Following growth, the graphene films were transferred onto degenerately doped Si substrates bearing a 100 nm thermally grown SiO_2 dielectric layer using a PMMA-assisted wet electrochemical delamination process. A PMMA solution (950 K molecular weight, 4.5 wt% in anisole, AR-P 672.045, All-Resist, Berlin, Germany) was spin-coated onto the Gr/Ge/Si stack at 4000 rpm for 90 s, yielding a mechanically robust polymer support layer approximately 410 nm in thickness. Following spin-coating, the PMMA film was allowed to dry at room temperature before the coated wafer was diced into 2 × 2 cm^2 pieces.

Electrochemical delamination [25], as systematically illustrated in Fig. 1, was carried out in a 0.3 M KOH aqueous electrolyte solution. In this configuration, the PMMA/Graphene/Ge/Si stack served as the working cathode, while a graphite plate acted as the counter anode. Upon application of a bias in the range of 3–5 V between electrodes, the exact value being adjusted according to lateral dimensions of the sample to ensure uniform bubble generation across the film, electrochemically generated H_2 gas bubbles nucleated preferentially at the PMMA/Gr–Ge interface, and delaminated the PMMA/Gr film from the Ge/Si substrate within 3–10 s, depending on the applied voltage and sample size. The free-floating PMMA/Gr membrane was carefully scooped from the electrolyte bath and rinsed multiple times in deionized water. The cleaned membrane was subsequently placed onto the target SiO_2/Si substrates, followed by bake at 130 °C for 4 h.

PMMA removal was subsequently carried out using a combination of a commercial two-component remover (AR 600–71, All-Resist, Berlin, Germany), comprising 70 vol% 1,3-dioxolane and 30 vol% 1,2-methoxypropanol, and standard acetone, applied in varying time sequences as listed in Table 1. Following solvent treatment, the sample was rinsed thoroughly in isopropanol (IPA) to remove residual solvent from the surface of graphene. The sample was finally dried under a gentle N_2 gas stream.

2.3. Characterisation

Surface morphology of transferred graphene films was characterized by atomic force microscopy operated in tapping mode (Dimension Icon, Bruker, Billerica, MA, USA). All AFM images were processed and analyzed using Gwyddion open-source software. The chemical composition of transferred graphene films was characterized by X-ray photoelectron spectroscopy (XPS) using a SPECS spectrometer (SPECS GmbH, Berlin, Germany) equipped with a monochromatic Al Kα X-ray source ($h\nu$ = 1486.6 eV). Spectral decomposition was performed following Shirley background subtraction, with individual components fitted using Gaussian–Lorentzian (Voigt) convolution line shapes for all chemical species. An exception was made for the sp^2-bonded graphene carbon component in the C 1 s spectrum, which was fitted using an asymmetric Lorentzian (LF) line shape.

Raman spectroscopy was performed using a 532 nm continuous-wave laser excitation source (inVia confocal Raman microscope, Renishaw, Wotton-under-Edge, UK) to assess the structural quality of transferred graphene films. Spatially resolved Raman mapping was performed over a representative 7 × 7 μm^2 area using a motorized sample stage with a step size of 1 μm, generating a grid of 49 spectra from which spatial maps of peak position, intensity, and width were extracted. All spectra were frequency-calibrated against the first-order optical phonon peak of the Si substrate at 520.4 cm^{-1} to correct for any instrumental drift between measurements.

3. Results and discussions

To evaluate the influence of solvent treatment time and sequence on PMMA residue removal efficiency, surface morphology of all transferred graphene samples was systematically investigated by AFM. A representative 5 × 5 μm^2 scan area was selected to enable statistically quantitative analysis of residual polymer surface coverage, particle size distribution, and topographic variations. In addition, 50 × 50 μm^2 scans were acquired for all samples to assess surface uniformity over a larger area, and these are provided in Supplementary Information (S1). To isolate graphene-related surface features from substrate contributions, a reference AFM scan was independently performed on a bare SiO_2/Si substrate prior to graphene transfer, establishing the intrinsic substrate roughness as a baseline for subsequent comparative analysis.

As shown in Fig. 2, for acetone-first treatment sequence, surface residue density decreases progressively from 3 *min* (T3) to 5 *min* (T5),

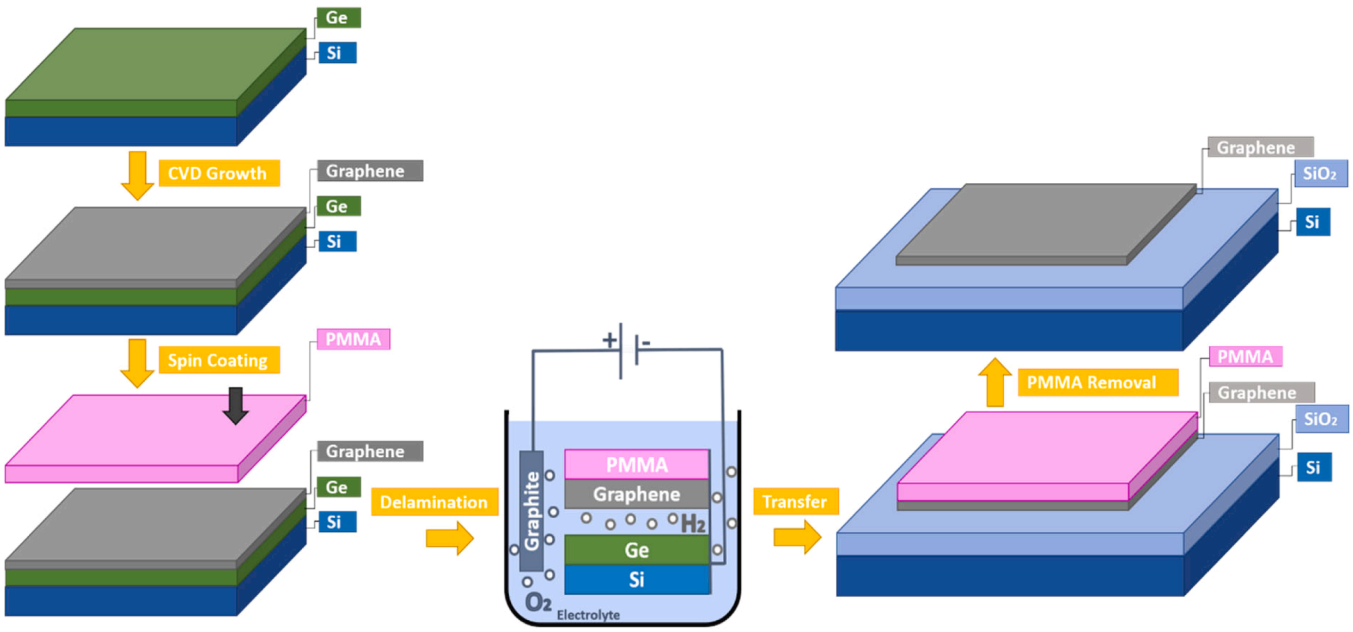


Fig. 1. Schematic illustration of the electrochemical bubbling transfer process of CVD graphene from Ge/Si growth substrates to a SiO_2/Si target substrate using a PMMA support layer and hydrogen bubble-assisted delamination in electrolyte solution.

Table 1
Solvent treatment conditions for PMMA removal for transferred graphene. T3-T10 denote treatment times of 3, 5, 7, and 10 min, respectively, applied equally to both solvent steps within each sequence.

		Acetone First		Remover First	
Sample	Time (min)	Step 1	Step 2	Step 1	Step 2
T3	3	Acetone	Remover	Remover	Acetone
T5	5	Acetone	Remover	Remover	Acetone
T7	7	Acetone	Remover	Remover	Acetone
T10	10	Acetone	Remover	Remover	Acetone

indicating effective dissolution and desorption of PMMA fragments from graphene surface within this initial time window. However, beyond 5 *min* (T5), residue density increases markedly through 7 *min* (T7) and 10 *min* (T10), accompanied by the emergence of large, irregularly distributed polymer particle clusters with lateral dimensions of approximately 2030 *nm*. An analogous trend is observed for remover-first sequence, where residue coverage similarly reaches a minimum at 5 *min* (T5) before increasing progressively at 7 *min* (T7) and 10 *min* (T10). This behavior is attributed to a solvent saturation mechanism; during initial treatment window, both acetone and remover effectively dissolve and desorb PMMA chain segments and nanoscale polymer clusters from graphene surface, reducing residue coverage with increasing immersion time. However, upon reaching solvent saturation concentration with dissolved PMMA, the thermodynamic driving force for further polymer dissolution diminishes, and continued immersion promotes redeposition and reaggregation of dissolved PMMA oligomers and fragments back onto the graphene surface from saturated solution due to evaporation of solvents [22,26], resulting in increasing residue coverage, larger aggregate particle sizes, and deteriorating surface quality at 7 *min* (T7) and 10 *min* (T10).

Surface RMS roughness values, extracted from five different 5 × 5 μm^2 AFM images and plotted as a function of treatment time and

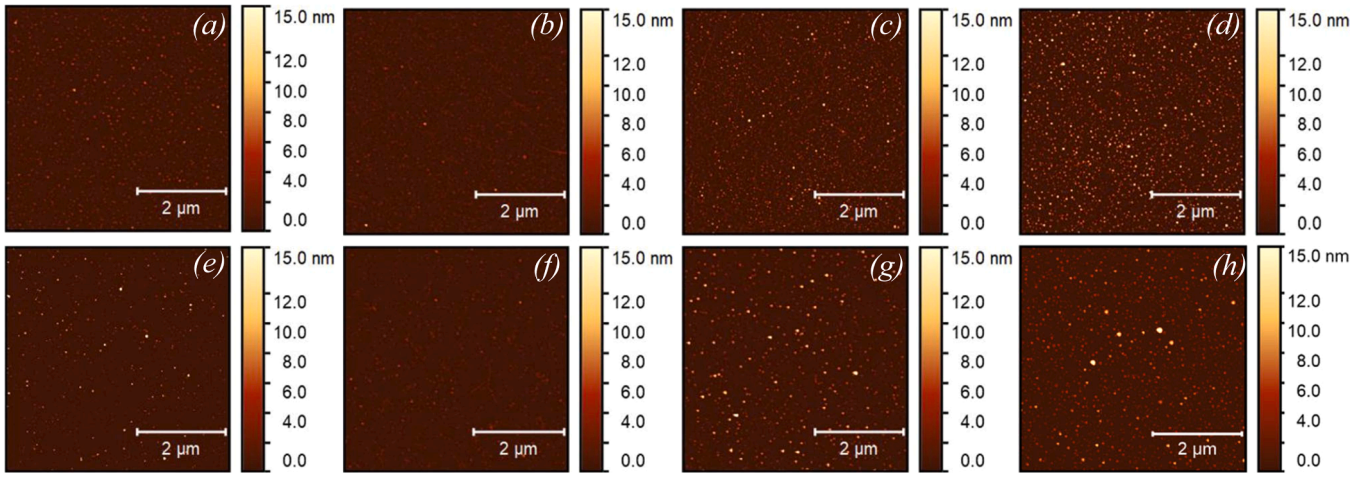


Fig. 2. AFM topography images (5 × 5 μm^2) of monolayer graphene transferred onto SiO_2/Si substrates following PMMA removal under varying solvent treatment times and sequences. **(a-d)** Acetone-first sequence at 3 (T3), 5 (T5), 7 (T7), and 10 (T10) min, respectively. **(e-h)** Remover-first sequence at 3 (T3), 5 (T5), 7 (T7), and 10 (T10) min, respectively. All images were acquired in tapping mode with an identical color scale ranging from 0 to 20 nm.

solvent sequence in Fig. 3, provides further evidence of this saturation behavior. For acetone-first series, RMS roughness decreases from 0.85 ± 0.06 *nm* at 3 *min* (T3) to 0.70 ± 0.05 *nm* at 5 *min* (T5), before sharply increasing to 1.40 ± 0.06 *nm* at 7 *min* (T7) and 2.05 ± 0.08 *nm* at 10 *min* (T10). For remover-first series, RMS roughness decreases from 0.80 ± 0.05 *nm* at 3 *min* (T3) to 0.54+0.05 nm at 5 *min* (T5); a value closely approaching the intrinsic RMS roughness of the bare SiO_2/Si substrate independently measured prior to transfer (0.49 *nm*) before increasing to 1.20 ± 0.07 *nm* at 7 *min* (T7) and 1.37 *nm* ± 0.06 at 10 *min* (T10). Furthermore, the number of particles were counted for all parameters. For acetone-first series, the number of particles decreases from 356 at 3 *min* (T3) to 63 at 5 *min* (T5), before gradually increasing to 1470 at 7 *min* (T7) and 2192 at 10 *min* (T10). For remover-first series, the number of particles decreases more substantially from 238 at 3*min* (T3) to a minimum of 56 at 5*min* (T5), before increasing to 508 at 7*min* (T7) and 1971 at 10 *min* (T10). These results collectively and unambiguously establish 5 *min* (T5) as the optimal treatment duration for both solvent sequences. Additionally, across all investigated treatment times, remover-first sequence consistently yields lower RMS roughness values and reduced residual particle count compared to acetone-first sequence, the detailed discussion is below.

To further assess surface uniformity over larger areas, optical microscopy images were acquired at a field of view of approximately 1000 μm for graphene cleaned with acetone alone and with optimized protocol, 5 *min* (T5) in Remover-first sequence, as demonstrated in Fig. 4a&b. Samples treated with acetone alone showed pronounced PMMA residue contamination, whereas optimized protocol substantially reduced residue coverage, yielding a clean and homogeneous graphene film.

To provide direct and quantitative chemical evidence of residue removal efficiency, and to complement morphological findings from AFM, XPS analysis of the C 1 s core-level spectra was performed for all treatment time and sequence conditions. Representative C 1 s spectra for the acetone-first and remover-first sequences are shown in Fig. 5. Spectral deconvolution was performed following Shirley background subtraction, with the sp^2-bonded graphene carbon component at 284.4 eV fitted using an asymmetric Lorentzian (LF) line shape to account for the intrinsic asymmetry arising from electron–hole pair excitations near the Fermi level, while all other chemical components including C—C/C—H at 285.7 eV, C═O at 288.0 eV, and O—C═O-carbonyl species at 290.1 eV associated with residual PMMA were fitted

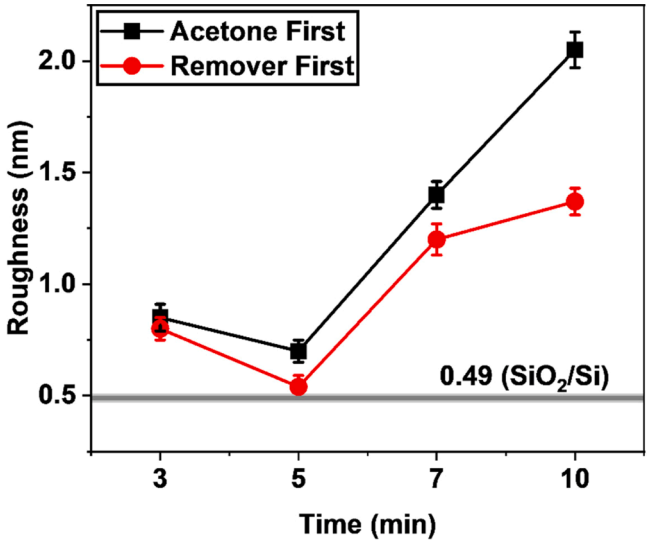


Fig. 3. RMS surface roughness of transferred graphene onto SiO_2/Si substrates as a function of solvent treatment time for acetone-first (black) and remover-first (red) sequences. The grey line denotes the intrinsic RMS roughness of bare SiO_2/Si.

with Gaussian–Lorentzian (Voigt) profiles [15,27–29]. The C—C/C—H component, which constitutes the dominant atomic concentration contribution of PMMA and is directly attributable to aliphatic backbone and methyl side-chain species of residual polymer fragments [29], was plotted as a function of treatment time for both sequences in Fig. 6a. For acetone-first series, the C—C/C—H concentration decreases from 11.69 *at*.% at 3 *min* (T3) to 8.18 *at*.% at 5 *min* (T5), before gradually increasing to 11.87 *at*.% at 7 *min* (T7) and 16.68 *at*.% at 10 *min* (T10), consistent with AFM-observed PMMA redeposition at extended treatment times. For remover-first series, the C—C/C—H concentration decreases more substantially from 8.6 *at*.% at 3*min* (T3) to a minimum of 3.2 *at*.% at 5*min* (T5), approaching the values of as-grown graphene on Ge/Si, 2.85 *at*.%, before increasing to 11.03 *at*.% at 7*min* (T7) and 13.15 *at*.% at 10 *min* (T10), indicating that remover-first protocol achieves higher residue removal at the optimal treatment time (T5), in agreement with AFM roughness and particle density findings.

Furthermore, surface concentration of C═O and O—C═O carbonyl species (%), which can be assigned to residual PMMA fragments retaining their ester side-chain functionality [29], was quantified as a function of treatment time and plotted for both sequences in Fig. 6b. For acetone-first series, the C═O concentration decreases sharply from 11.83 *at*. % at 3 *min* (T3) to 9.29 *at*. % at 5 *min* (T5), confirming significant PMMA removal within the optimal treatment time, before recovering progressively to 15.91 *at*. % at 7 *min* (T7) and 21.79 *at*. % at 10 *min* (T10). For remover-first series, the C═O and O—C═O concentration decreases from 11.81 *at*. % at 3 *min* (T3) to approximately 6.77 *at*. % at 5 *min* (T5), with increase to 14.25 *at*. % at 7 *min* (T7) and 19.33 *at*. % at 10 *min* (T10). The complete elimination of O-C═O *at*. % and lowest *at*. % of C═O carbonyl species at T5 remover-first condition in stark contrast to the residual 9.29 *at*.% retained under acetone-first T5 condition provides chemical evidence that remover-first protocol at optimal treatment time achieves the most thorough PMMA residue removal among all conditions investigated.

The experimentally observed differences in cleaning efficiency between acetone and AR 600–71 remover can be rationalized within a thermodynamic framework based on Flory–Huggins polymer solution theory in conjunction with three-dimensional Hansen solubility parameter (HSP) analysis. Within the Flory–Huggins mean-field framework, the Gibbs free energy of mixing (ΔF_{mix}) per lattice site for a polymer–solvent binary system is expressed as [30]:

$$\frac{\Delta F_{mix}}{KT} = n_1 \ln v_1 + n_2 \ln n_2 + \chi_{12} n_1 v_2 \quad (1)$$

Where, K is the Boltzmann constant, T is the absolute temperature, n_1 and n_2 are the number of solvent and polymer molecules, respectively, v_1 and v_2 are the corresponding volume fractions satisfying $v_1 + v_2 = 1$, and χ_{12} is the dimensionless Flory–Huggins interaction parameter that quantifies the net enthalpic interaction between solvent and polymer segments. Spontaneous dissolution requires $\Delta F_{mix} < 0$, and for a fixed polymer molecular weight, a lower value of χ_{12} corresponds to a greater thermodynamic driving force for dissolution [31]. For polar solvent–polymer systems, χ_{12} is estimated from the solubility parameter components as [30]:

$$\chi_{12} = \frac{V_1 A_{1,2}}{RT} \quad (2)$$

where V_1 is the molar volume of the solvent, R is the universal gas constant, and $A_{1,2}$ is the Hildebrand solubility interaction term defined in terms of the three independent HSP components: dispersive (δ_D), polar (δ_P), and hydrogen-bonding (δ_H) according to[31,32]:

$$A_{1,2} = \left[(\delta_{D2} - \delta_{D1})^2 + 0.25(\delta_{P2} - \delta_{P1})^2 + 0.25(\delta_{H2} - \delta_{H1})^2\right] \quad (3)$$

The HSP values for all solvent components and PMMA are compiled in Table 2 [30–32]. The calculated χ_{12} values confirm that AR 600–71

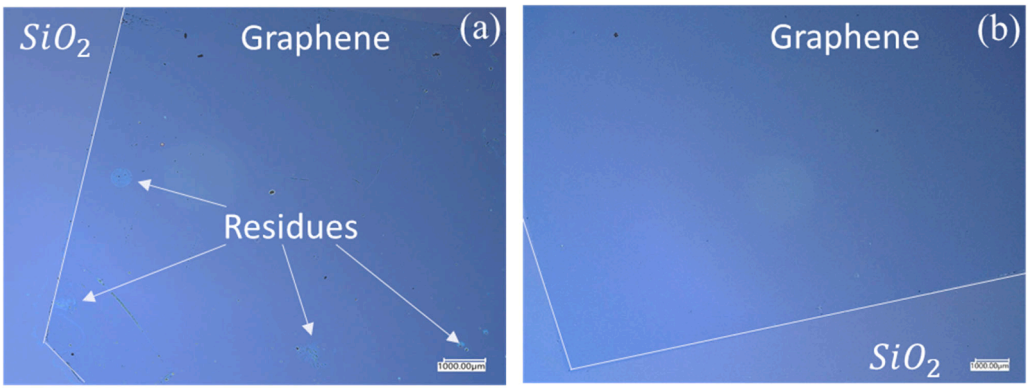


Fig. 4. Optical microscopy images of transferred graphene on SiO_2/Si. **(a)** Graphene cleaned with acetone alone, showing PMMA residues. **(b)** Graphene cleaned with optimized protocol, showing substantially reduced residues and a clean, uniform film.

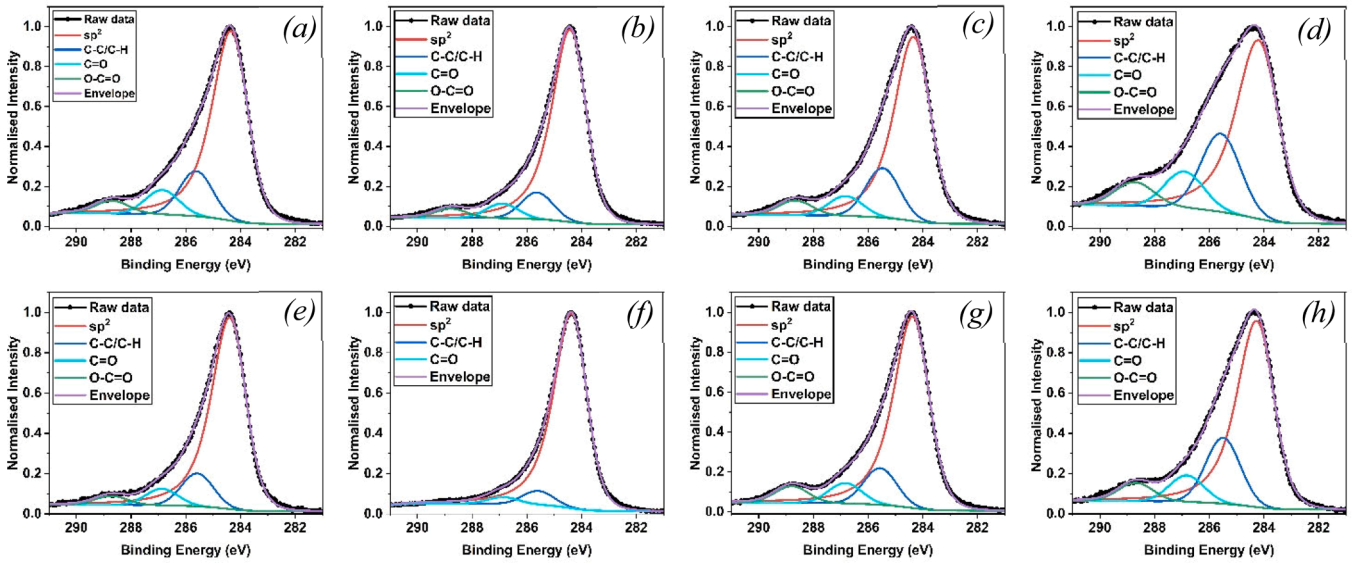


Fig. 5. XPS Carbon 1 s core level of varying solvent treatment times and sequences. **(a-d)** Acetone-first sequence at 3 (T3), 5 (T5), 7 (T7), and 10 (T10) min, respectively. **(e-h)** Remover-first sequence at 3 (T3), 5 (T5), 7 (T7), and 10 (T10) min, respectively.

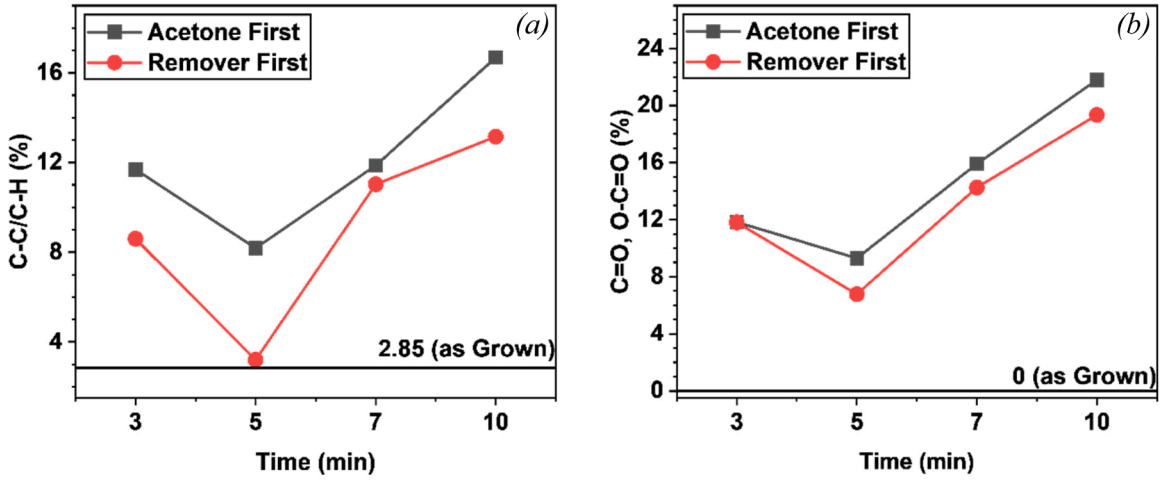


Fig. 6. **(a)** C—C/C—H area concentration (%) and **(b)** C═O and O—C═O area concentration (%) extracted from C 1 s core-level spectra for acetone-first (black) and remover-first (red) as a function of solvent treatment time. The black lines denote the values of at % for as-grown graphene on Ge/Si.

remover (χ_{12} = 0.22) exhibits substantially greater thermodynamic affinity for PMMA than acetone (χ_{12} = 0.28), providing a quantitative

Table 2
Molar Volumes, three-dimensional solubility parameters, Flory-Huggins interaction parameters for solvents acetone, remover and its components are provided.

	$V(cm^3/mol)$	$\delta_d[(MPa)^{1/2}]$	$\delta_P[(MPa)^{1/2}]$	$\delta_H[(MPa)^{1/2}]$	χ_{12}	H
Acetone	74.01	15.5	10.4	7.0	0.28	0.72
Remover	78.18	17.35	6.51	9.99	0.22	0.61
1,2-MethoxyPropanol	97.5	15.6	6.3	11.6	0.08	1.12
1,3-Dioxolane	69.9	18.1	6.6	9.3	0.23	0.39

thermodynamic basis for the experimentally observed superior dissolution performance of the remover. To further characterize solvent–polymer thermodynamic compatibility within the HSP framework, the Hansen solubility distance R_a between solvent and polymer was calculated according to the Skaarup equation [30]:

$$(R_a)^2 = 4(\delta_{D2} - \delta_{D1})^2 + (\delta_{P2} - \delta_{P1})^2 + (\delta_{H2} - \delta_{H1})^2 \quad (4)$$

The relative energy difference parameter H, normalized by the HSP sphere radius (R_M) and distance in Hansen space (R_A), defined as the maximum tolerable solubility parameter difference within which the polymer remains soluble is expressed as [30]:

$$H = \frac{(R_A)^2}{(R_M)^2} = \frac{(\delta_{D2} - \delta_{D1})^2 + (\delta_{P2} - \delta_{P1})^2/4 + (\delta_{H2} - \delta_{H1})^2/4}{(R_M)^2} \quad (5)$$

Where, $R_A = R_a/2$ and $R_M = R_0/2$. The parameter H equals zero when the solvent and polymer solubility parameters are perfectly matched, representing ideal solvation conditions, and increases monotonically as thermodynamic incompatibility grows. Dissolution is thermodynamically favorable when $R_A < R_M$, corresponding to $H < 1$, while $H > 1$ indicates a non-solvent [30]. As summarized in Table 2, $H_{\frac{acetone}{PMMA}} = 0.72$ and $H_{\frac{Remover}{PMMA}} = 0.61$, confirming that AR 600–71 remover lies significantly closer to the center of the PMMA solubility sphere than acetone, and therefore constitutes a thermodynamically superior solvent for PMMA dissolution. Taken together, both the χ_{12} and H parameters provide a consistent and quantitative thermodynamic rationale for the experimentally observed superiority of remover-first cleaning protocol.

Structural quality, defect density, charge doping level, and strain state of the transferred graphene films under all treatment conditions were characterized by Raman spectroscopy, which provides a non-destructive, highly sensitive probe of graphene's electronic and phonon structure. Raman mapping was performed over a $7 \times 7\ \mu m^2$ area with a 1 μm step size, yielding 49 spatially resolved spectra per sample, all of which were fitted with Gaussian–Lorentzian line profiles following baseline correction to extract D, G, and 2D band positions, intensities, and linewidths with high statistical reliability. representative spectra with characteristic D, G and 2D peaks, for both treatment sequences across all time conditions are illustrated in Fig. 7.

The D-to-G band intensity ratio, I(D)/I(G), is a widely employed metric for quantifying the density of sp^3-type lattice defects and disorder in graphene, with contributions arising from grain boundaries, transfer-induced structural damage such as tears and folds, and surface adsorbates that locally perturb the graphene lattice symmetry and activate the otherwise Raman-inactive D band through intervalley double-resonance scattering [33–35]. As shown in Fig. 8a, for acetone-first series, I(D)/I(G) decreases from 0.8 ± 0.08 at 3 *min* (T3) to 0.4 ± 0.04 at 5 *min* (T5), indicating a reduction in adsorbate-induced disorder with improved residue removal at the optimal treatment time, before increasing to 0.62 ± 0.06 at 7 *min* (T7) and 0.83 ± 0.15 at 10 *min* (T10), consistent with the redeposition of PMMA fragments introducing additional scattering sites at extended immersion durations. For remover-first series, I(D)/I(G) decreases from 0.55 ± 0.06 at 3 *min* (T3) to 0.39 ± 0.02 at 5 *min* (T5); closely approaching the I(D)/I(G) value of 0.22 ± 0.04, measured for as-grown graphene on Ge/Si, indicative of near-complete removal of transfer- and adsorbate-induced disorder, consistent with AFM and XPS findings before recovering to 0.51 ± 0.07 at 7 *min* (T7) and 0.53 ± 0.09 at 10 *min* (T10).

The 2D-to-G band intensity ratio, (I(2D)/I(G)), provides information on charge doping state of graphene. Charge transfer from surface adsorbates shifts the graphene Fermi level away from the Dirac point, which modifies the electron–phonon coupling matrix elements governing the relative intensities of the G and 2D bands, resulting in a suppression of I(2D)/I(G) with increasing carrier concentration [23,34,34,36–38]. As shown in Fig. 8b, for acetone-first series, I(2D)/I(G) increases from 2.89 ± 0.07 at 3 *min* (T3) to 3.2 ± 0.06 at 5 *min* (T5), indicating a reduction in adsorbate-induced charge transfer doping at the optimal cleaning time, before decreasing to 2.96 ± 0.05 at 7 *min* (T7) and 2.52 ± 0.07 at 10 *min* (T10), consistent with increasing doping from redeposited PMMA at extended treatment times. For remover-first series, I(2D)/I

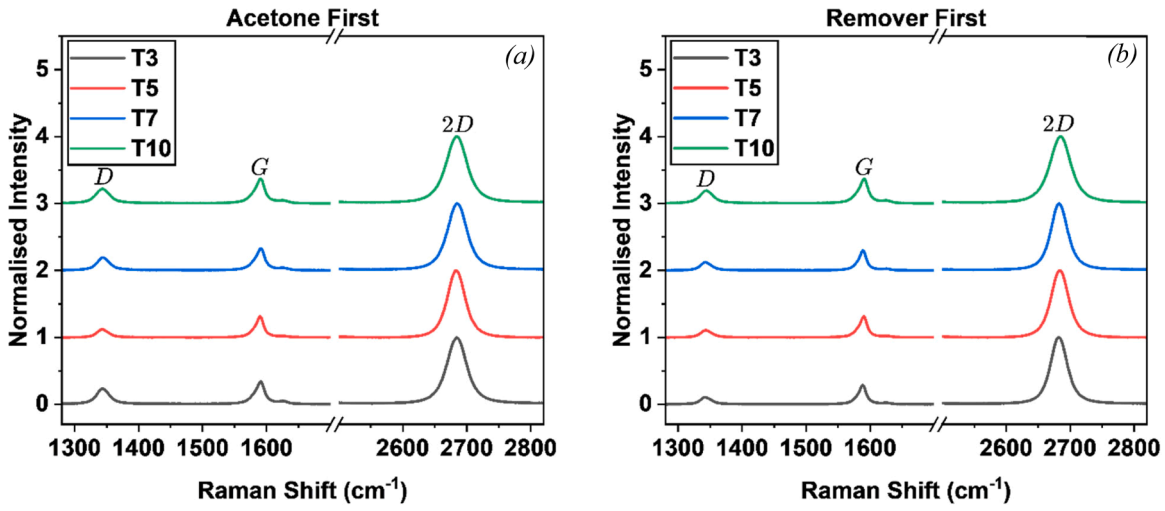


Fig. 7. Representative Raman spectra of transferred graphene onto SiO_2/Si substrates at treatment times 3 min (T3), 5 min (T5), 7 min (T7), and 10 min (T10) for **(a)** acetone-first and **(b)** remover-first.

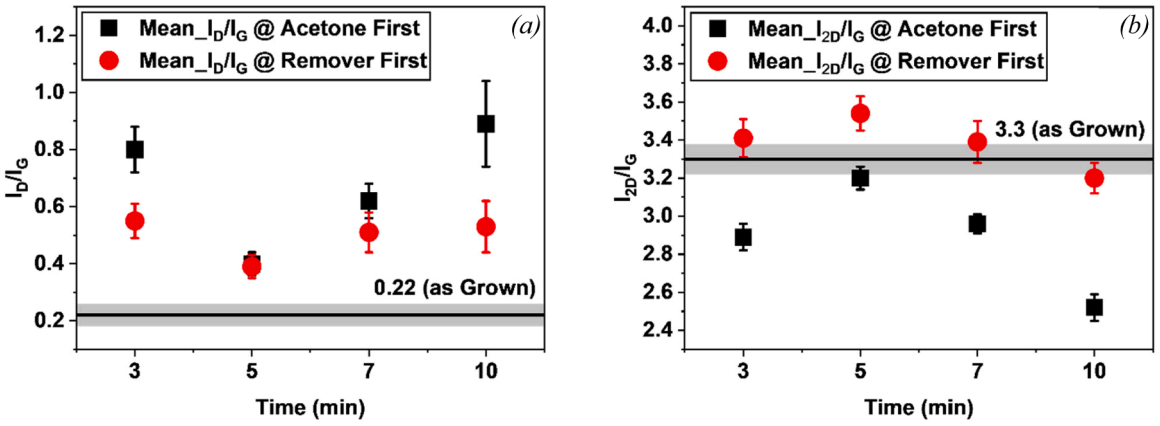


Fig. 8. Raman peak intensity ratios of transferred graphene onto SiO_2/Si substrates as a function of solvent treatment time and sequence. **(a)** I_D/I_G and **(b)** I_{2D}/I_G ratios for acetone-first (black) and remover-first (red) sequences. The black line denotes the values of as-grown graphene on Ge/Si.

(G) increases more substantially from 3.41 ± 0.1 at 3 *min* (T3) to 3.54 ± 0.09 at 5 *min* (T5) exceeding 3.3 ± 0.08, the value characteristic of as-grown graphene on Ge/Si, indicating near-complete elimination of transfer-induced doping before decreasing to 3.39 ± 0.11 at 7 *min* (T7) and 3.2 ± 0.08 at 10 *min* (T10) as PMMA redeposition progressively re-introduces charge transfer centers.

Carrier doping concentrations and biaxial strain were independently and simultaneously quantified by analyzing the correlation between the 2D and G band peak positions, as shown in Fig. 9. In this representation, variations along the strain axis primarily reflect shifts in both peak positions due to phonon renormalization under mechanical deformation, while deviations along doping axis reflect asymmetric shifts driven by Fermi level-dependent electron–phonon coupling [34,36,39–44]. For acetone-first series, as illustrated in Fig. 9a, the extracted carrier concentration decreases from 0.5 × 10^{13} cm^{-2} at 3 *min* (T3) to 0.3 × 10^{13} cm^{-2} at 5 *min* (T5), before increasing to 0.6 × 10^{13} cm^{-2}at 7 *min* (T7) and 0.58 × 10^{13} cm^{-2} at 10 *min* (T10). For remover-first series, as illustrated in Fig. 9b, the carrier concentration for 3 *min* (T3) and 5 *min* (T5) is overlapping at 0.29 × 10^{13} cm^{-2}, marginally below the as-grown doping value of 0.5 × 10^{13} cm^{-2} measured on Ge/Si before increasing to 0.4 × 10^{13} cm^{-2} at 7 *min* (T7) and 0.5 × 10^{13} cm^{-2} at 10 *min* (T10). The slightly lower doping value at T5 in remover-first series compared to the as-grown reference is attributed to the absence of Ge substrate-induced charge transfer on the insulating SiO_2/Si target substrate, where substrate-graphene electrostatic coupling is negligible, in contrast to semiconducting Ge growth substrate where residual substrate-mediated doping contributions are present [45–47]. The minimum doping at T5 in both sequences, and the consistently lower absolute doping values throughout the remover-first series compared to the acetone-first series, are in full quantitative agreement with the I (2D)/I(G) trends and the XPS C═O concentration data, collectively confirming that residual carbonyl-containing PMMA molecular species constitute the primary and dominant source of unintentional charge doping in the transferred graphene films under all treatment conditions investigated. Strain analysis derived from the 2D–G peak position correlation plot provides additional mechanistic insight into the influence of surface residues on the mechanical state of transferred graphene. For acetone-first series, as shown in Fig. 9a, a slight compressive strain of −0.01% at 3 *min* (T3) transitions to weak tensile strain of +0.009% at 5 *min* (T5), which increases progressively to +0.01% at 7 *min* (T7) and +0.03% at 10 *min* (T10). For remover-first series, as shown in Fig. 9b, a compressive strain of −0.04% at 3 *min* (T3) decreases in magnitude to approximately 0% at 5 *min* (T5), with residual compressive values of −0.03% at 7 *min* (T7) and −0.01% at 10 *min* (T10). Although no dominant monotonic strain trend is observed across all conditions, the near-zero strain measured at the T5 remover-first condition is physically significant and consistent with the nearly complete residue removal established by AFM and XPS. The progressive development of tensile strain at extended treatment times in the acetone-first series is attributed to the preferential interaction between the graphene

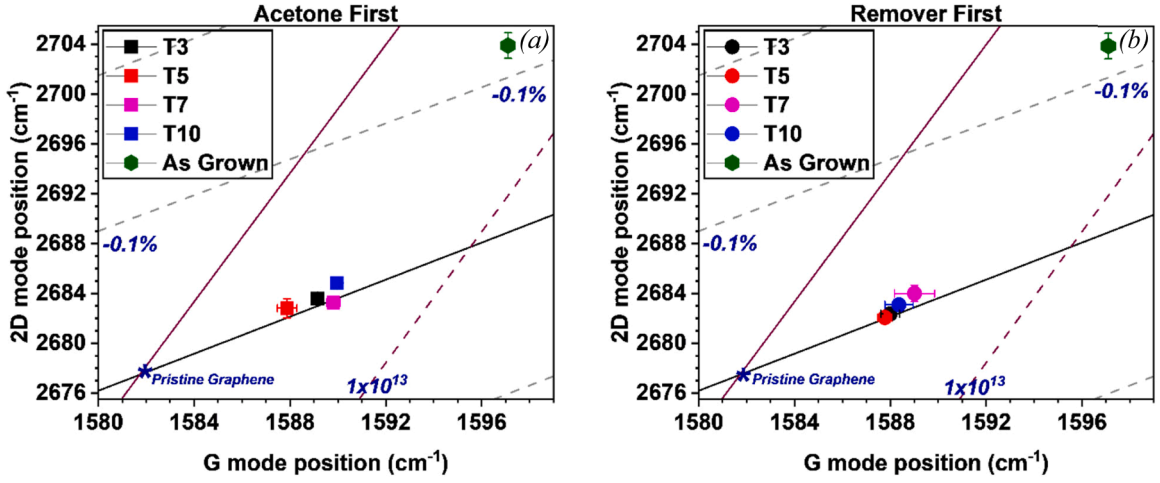


Fig. 9. Correlation analysis of 2D and G frequencies to separate the frequency shifts from strain and doping. The plots illustrate the doping and strain variation **(a)** for acetone-first sequence and **(b)** for remover-first at varied times (3 min (T3)-10 min (T10)).

π-electron system and redeposited PMMA fragments, driven by the closely matched Hildebrand solubility parameters of graphene ($\sim 22.7\ MPa^{1/2}$) and PMMA ($\sim 23\ MPa^{1/2}$) [48,49]. This near-identical solubility parameter match implies a strong thermodynamic affinity between graphene and PMMA relative to SiO_2, promoting preferential PMMA adsorption on graphene domains and generating local tensile strain fields as the adsorbed polymer chains contract upon drying and impose lateral mechanical forces on the underlying graphene lattice.

The FWHM of the 2D band, which is sensitive to local strain inhomogeneity within the laser spot area arising from spatially non-uniform residue distribution and substrate-induced corrugation, serves as a reliable and quantitative indicator of the overall structural quality and strain homogeneity of on-substrate graphene layers [23,34,37,50,51]. As shown in Fig. 10, for acetone-first series, FWHM(2D) decreases from $37.09 \pm 0.36\ cm^{-1}$ at 3 *min* (T3) to $33.44 \pm 0.15\ cm^{-1}$at 5 *min* (T5), before increasing to $37.81 \pm 0.21\ cm^{-1}$ at 7 *min* (T7) and $38.12 \pm 0.64\ cm^{-1}$ at 10 *min* (T10). For remover-first series, FWHM (2D) decreases from $32.04 \pm 0.39\ cm^{-1}$ at 3 *min* (T3) to $31.29 \pm 0.19\ cm^{-1}$at 5 *min* (T5) closely matching the FWHM(2D) value of as-grown graphene on Ge/Si, $30.28 \pm 0.19\ cm^{-1}$, indicating minimal strain inhomogeneity and high structural quality before increasing to $33.08 \pm 0.58\ cm^{-1}$at 7 *min* (T7) and $36.36 \pm 0.61\ cm^{-1}$ at 10 *min* (T10). The minimum FWHM(2D) at T5 in remover-first series, approaching the as-grown reference value, confirms that the optimized cleaning conditions produce transferred graphene films with lowest strain fluctuations and highest structural homogeneity achievable under the investigated processing conditions, fully consistent with the near-complete residue removal established by complementary AFM and XPS analyses.

It is important to note that while the remover-first protocol delivers comprehensively superior cleaning performance across all characterization metrics, AR 600–71 remover alone is insufficient for complete PMMA removal after the transfer of graphene. As demonstrated in the supporting information (S2), Raman spectra acquired after remover-only treatment exhibit additional vibrational features beyond the characteristic D, G, and 2D bands of graphene, attributed to residual molecular species originating from the remover formulation itself [52], specifically adsorbed 1,3-dioxolane or 1,2-methoxypropanol molecules retained on the graphene surface after the treatment. This observation has a critical practical implication: acetone is indispensable not only for dissolving any remaining PMMA fragments that the remover treatment leaves behind, but also for removing remover-derived molecular residues from the graphene surface. The combined and sequential application of AR 600–71 remover followed by acetone at the optimized treatment time T5 is therefore necessary and sufficient to achieve a clean, electronically undisturbed graphene surface after transfer, and neither solvent alone can fulfill this requirement.

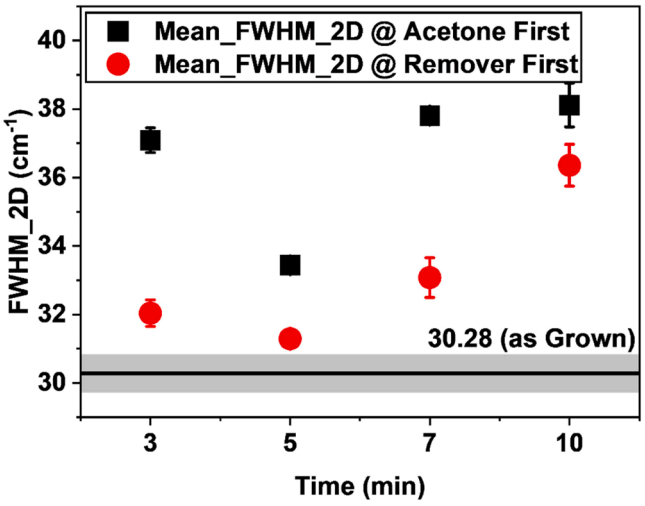


Fig. 10. FWHM of the 2D band extracted from Raman mapping of transferred graphene onto SiO_2/Si substrates as a function of solvent treatment time for acetone-first (black) and remover-first (red) sequences. The black line denotes the values of as-grown graphene on Ge/Si.

To assess the reproducibility and broader applicability of optimized cleaning protocol, complete transfer and cleaning procedure was repeated on 15 independently prepared samples, using monolayer graphene grown on both Ge(110)/Si and Ge(001)/Si substrates and transferred onto SiO_2/Si under equivalent experimental conditions. Representative results from one Ge(110)/Si sample are presented here, and corresponding results for Ge(001)/Si are provided in the Supplementary Information (S3). Comprehensive AFM, XPS, and Raman characterization of all samples yielded consistent results across every treatment time and sequence condition. In both cases, T5 remained the optimal treatment duration, and remover-first sequence consistently provided superior cleaning. This was further confirmed by 10 additional tests at T5 comparing acetone-first and remover-first sequences, which reproduced sequence-dependent result. These findings demonstrate that while surface orientation of Ge growth substrate plays a significant role in determining the nucleation density, domain size, and structural properties of CVD-grown graphene during synthesis, it exerts no measurable influence on the adhesion characteristics of graphene film to the PMMA support layer, the electrochemical delamination dynamics, or the post-transfer cleaning behavior on SiO_2/Si substrates. The cleaning protocol established in this work is therefore universally applicable to PMMA-assisted wet transfer of CVD graphene grown on Ge/Si substrates of any crystallographic orientation, providing a robust and transferable processing standard for CMOS-compatible graphene device integration. Complete characterization data for Ge(001)/Si samples are provided in supporting information.

4. Conclusion

In Conclusion, we have systematically investigated the effect of solvent treatment time and sequence on PMMA residue removal from wafer-scale CVD graphene grown on Ge(110)/Si substrates and transferred onto SiO_2/Si via electrochemical delamination-assisted wet transfer. AFM, XPS, and Raman spectroscopy consistently identified 5 *min* (T5) as optimal treatment duration in both solvent sequences, beyond which PMMA redeposition from the polymer-saturated solvent bath progressively deteriorates surface cleanliness. Remover-first sequence outperformed acetone-first approach across all treatment times and characterization metrics, achieving an RMS roughness approaching the intrinsic SiO_2/Si substrate value, near-complete elimination of PMMA-associated C—C/C—H species, and Raman parameters recovering to as-grown graphene values at T5. The superior performance of AR 600–71 remover was understood thermodynamically through lower Flory–Huggins interaction parameter ($\chi_{12} = 0.22$) and relative energy difference ($H = 0.61$) values compared to acetone (($\chi_{12} = 0.28$), ($H = 0.68$)), confirming its greater thermodynamic affinity for PMMA dissolution. The combined sequential application of remover followed by acetone at T5 was established as both necessary and sufficient for optimum cleaning, as neither solvent alone achieves complete residue removal. These findings provide clear and actionable guidelines for optimizing PMMA removal in large-scale graphene transfer, directly relevant to CMOS-compatible graphene device integration.

Funding

This project has received funding from the European Union's Horizon Europe research and innovation programme under grant agreement No 101120938 (GATEPOST) and under grant agreement 101189797 (2D-PL).

Generative AI usage

No AI tools have used in this manuscript.

CRediT authorship contribution statement

Monika Choudhary: Writing – original draft, Validation, Investigation, Conceptualization. **Rasuole Lukose:** Writing – review & editing, Investigation. **Moriom Akter:** Writing – review & editing, Investigation. **Christian Wenger:** Writing – review & editing. **Mindaugas Lukosius:** Writing – review & editing, Supervision, Funding acquisition, Conceptualization.

Declaration of competing interest

The authors declare that they have no known competing financial interests or personal relationships that could have appeared to influence the work reported in this paper.

Supplementary materials

Supplementary material associated with this article can be found, in the online version, at doi:10.1016/j.cartre.2026.100716.

Data availability

Data will be made available on request.

References

[1] M. Lisker, M. Lukosius, R. Lukose, C. Wenger, A. Mai, *(Invited)* Challenges of graphene process integration in CMOS technology, ECS Trans 92 (2019) 201–210, https://doi.org/10.1149/09204.0201ecst.

[2] A. Mai, M. Lisker, M. Lukosius, G. Lupina, (Invited) Large scale graphene integration for Silicon technologies, ECS Trans 79 (2017) 3–10, https://doi.org/10.1149/07901.0003ecst.

[3] I. Pasternak, M. Wesolowski, I. Jozwik, M. Lukosius, G. Lupina, P. Dabrowski, J. M. Baranowski, W. Strupinski, Graphene growth on Ge(100)/Si(100) substrates by CVD method, Sci. Rep. 6 (2016) 21773, https://doi.org/10.1038/srep21773.

[4] F. Akhtar, J. Dabrowski, R. Lukose, C. Wenger, M. Lukosius, Chemical vapor deposition growth of graphene on 200 mm Ge(110)/Si wafers and ab initio analysis of differences in growth mechanisms on Ge(110) and Ge(001), ACS Appl. Mater. Interfaces 15 (2023) 36966–36974, https://doi.org/10.1021/acsami.3c05860.

[5] I. Pasternak, P. Dabrowski, P. Ciepielewski, V. Kolkovsky, Z. Klusek, J. M. Baranowski, W. Strupinski, Large-area high-quality graphene on Ge(001)/Si (001) substrates, Nanoscale 8 (2016) 11241–11247, https://doi.org/10.1039/C6NR01329E.

[6] I. Cheliotis, I. Zergioti, A review on transfer methods of two-dimensional materials, 2D Mater 11 (2024) 022004, https://doi.org/10.1088/2053-1583/ad2f43.

[7] S. Ullah, X. Yang, H.Q. Ta, M. Hasan, A. Bachmatiuk, K. Tokarska, B. Trzebicka, L. Fu, M.H. Rummeli, Graphene transfer methods: a review, Nano Res. 14 (2021) 3756–3772, https://doi.org/10.1007/s12274-021-3345-8.

[8] Y. Song, W. Zou, Q. Lu, L. Lin, Z. Liu, Graphene transfer: paving the road for applications of chemical vapor deposition Graphene, Small 17 (2021) 2007600, https://doi.org/10.1002/smll.202007600.

[9] G. Huang, R. Chen, M. Chen, X. Chen, M. Jiang, Y. Xing, J. Wang, B. Liang, Q. Liu, X. Li, C.S. Lau, X. Dong, P. Agarwal, L. Ke, S.M. Assad, J.-R. Soh, J. Lourembam, Y.-W. Cho, Q. Liang, J. Li, X. Zhang, Y. Ma, Y. Lu, P.K. Lam, X. Ma, Transfer and beyond: emerging strategies and trends in two-dimensional material device fabrication, Chem. Soc. Rev. 55 (2026) 2574–2634, https://doi.org/10.1039/D5CS00531K.

[10] P.V. Pham, T.-H. Mai, S.P. Dash, V. Biju, Y.-L. Chueh, D. Jariwala, V. Tung, Transfer of 2D films: from imperfection to perfection, ACS Nano 18 (2024) 14841–14876, https://doi.org/10.1021/acsnano.4c00590.

[11] Y. Gao, J. Chen, G. Chen, C. Fan, X. Liu, Recent progress in the transfer of graphene films and nanostructures, Small Methods 5 (2021) 2100771, https://doi.org/10.1002/smtd.202100771.

[12] A. Pirkle, J. Chan, A. Venugopal, D. Hinojos, C.W. Magnuson, S. McDonnell, L. Colombo, E.M. Vogel, R.S. Ruoff, R.M. Wallace, The effect of chemical residues on the physical and electrical properties of chemical vapor deposited graphene transferred to SiO2, Appl. Phys. Lett. 99 (2011) 122108, https://doi.org/10.1063/1.3643444.

[13] J. Kang, D. Shin, S. Bae, B.H. Hong, Graphene transfer: key for applications, Nanoscale 4 (2012) 5527, https://doi.org/10.1039/c2nr31317k.

[14] C.-D. Liao, A. Capasso, T. Queiros, T. Domingues, F. Cerqueira, N. Nicoara, J. Borme, P. Freitas, P. Alpuim, Optimizing PMMA solutions to suppress contamination in the transfer of CVD graphene for batch production, (2022).

[15] W. Xie, L.-T. Weng, K.M. Ng, C.K. Chan, C.-M. Chan, Clean graphene surface through high temperature annealing, Carbon 94 (2015) 740–748, https://doi.org/10.1016/j.carbon.2015.07.046.

[16] K. Kumar, Y.-S. Kim, E.-H. Yang, The influence of thermal annealing to remove polymeric residue on the electronic doping and morphological characteristics of graphene, Carbon 65 (2013) 35–45, https://doi.org/10.1016/j.carbon.2013.07.088.

[17] Y.-C. Lin, C.-C. Lu, C.-H. Yeh, C. Jin, K. Suenaga, P.-W. Chiu, Graphene annealing: how clean can it Be? Nano Lett. 12 (2012) 414–419, https://doi.org/10.1021/nl203733r.

[18] A.M. Goossens, V.E. Calado, A. Barreiro, K. Watanabe, T. Taniguchi, L.M. K. Vandersypen, Mechanical cleaning of graphene, Appl. Phys. Lett. 100 (2012) 073110, https://doi.org/10.1063/1.3685504.

[19] N. Lindvall, A. Kalabukhov, A. Yurgens, Cleaning graphene using atomic force microscope, J. Appl. Phys. 111 (2012) 064904, https://doi.org/10.1063/1.3695451.

[20] W. Choi, M.A. Shehzad, S. Park, Y. Seo, Influence of removing PMMA residues on surface of CVD graphene using a contact-mode atomic force microscope, RSC Adv 7 (2017) 6943–6949, https://doi.org/10.1039/C6RA27436F.

[21] S. Achra, T. Akimoto, J.-F. de Marneffe, S. Sergeant, X. Wu, T. Nuytten, S. Brems, I. Asselberghs, Z. Tokei, K. Ueno, M. Heyns, Enhancing interface doping in graphene-metal hybrid devices using H2 plasma clean, Appl. Surf. Sci. 538 (2021) 148046, https://doi.org/10.1016/j.apsusc.2020.148046.

[22] B. Zhuang, S. Li, S. Li, J. Yin, Ways to eliminate PMMA residues on graphene —— Superclean graphene, Carbon 173 (2021) 609–636, https://doi.org/10.1016/j.carbon.2020.11.047.

[23] A. Tyagi, V. Mišeikis, L. Martini, S. Forti, N. Mishra, Z.M. Gebeyehu, M.A. Giambra, J. Zribi, M. Frégnaux, D. Aureau, M. Romagnoli, F. Beltram, C. Coletti, ultra-clean high-mobility graphene on technologically relevant substrates, Nanoscale 14 (2022) 2167–2176, https://doi.org/10.1039/D1NR05904A.

[24] Y. Kim, H. Kim, T.Y. Kim, S.H. Rhyu, D.S. Choi, W.K. Park, C.-M. Yang, D.H. Yoon, W.S. Yang, Influence of the transfer and chemical treatment of monolayer graphene grown for flexible transparent electrodes, Carbon 81 (2015) 458–464, https://doi.org/10.1016/j.carbon.2014.09.078.

[25] C.J.L. de la Rosa, J. Sun, N. Lindvall, M.T. Cole, Y. Nam, M. Löffler, E. Olsson, K.B. K. Teo, A. Yurgens, Frame assisted H2O electrolysis induced H2 bubbling transfer of large area graphene grown by chemical vapor deposition on Cu, Appl. Phys. Lett. 102 (2013) 022101, https://doi.org/10.1063/1.4775583.

[26] X. Wang, A. Dolocan, H. Chou, L. Tao, A. Dick, D. Akinwande, C.G. Willson, Direct observation of poly(Methyl Methacrylate) removal from a graphene surface, Chem. Mater. 29 (2017) 2033–2039, https://doi.org/10.1021/acs.chemmater.6b03875.

[27] T.R. Gengenbach, G.H. Major, M.R. Linford, C.D. Easton, Practical guides for x-ray photoelectron spectroscopy (XPS): interpreting the carbon 1s spectrum, J. Vac. Sci. Technol. Vac. Surf. Films 39 (2021) 013204, https://doi.org/10.1116/6.0000682.

[28] A. Kovtun, D. Jones, S. Dell'Elce, E. Treossi, A. Liscio, V. Palermo, Accurate chemical analysis of oxygenated graphene-based materials using X-ray photoelectron spectroscopy, Carbon 143 (2019) 268–275, https://doi.org/10.1016/j.carbon.2018.11.012.

[29] C. Ton-That, A.G. Shard, D.O.H. Teare, R.H. Bradley, XPS and AFM surface studies of solvent-cast PS/PMMA blends, Polymer 42 (2001) 1121–1129, https://doi.org/10.1016/S0032-3861(00)00448-1.

[30] C.M. Hansen, Hansen Solubility Parameters: a User's Handbook, CRC Press, Boca Raton, Fla, 2000.

[31] Q. Hang, D.A. Hill, G.H. Bernstein, Efficient removers for poly (methylmethacrylate), J. Vac. Sci. Technol. B Microelectron. Nanometer Struct. Process. Meas. Phenom. 21 (2003) 91–97, https://doi.org/10.1116/1.1532734.

[32] (n.d.). https://stenutz.eu/chem/solv6%20(2).php?name=1-methoxy-2-propanol.

[33] C. Casiraghi, S. Pisana, K.S. Novoselov, A.K. Geim, A.C. Ferrari, Raman fingerprint of charged impurities in graphene, Appl. Phys. Lett. 91 (2007) 233108, https://doi.org/10.1063/1.2818692.

[34] A.K. Ott, A.C. Ferrari, Raman spectroscopy of graphene and related materials, Encycl. Condens. Matter Phys. (2024) 233–247, https://doi.org/10.1016/B978-0-323-90800-9.00252-3.

[35] J. Liu, Q. Li, Y. Zou, Q. Qian, Y. Jin, G. Li, K. Jiang, S. Fan, The dependence of graphene Raman D-band on carrier density, Nano Lett. 13 (2013) 6170–6175, https://doi.org/10.1021/nl4035048.

[36] Y. Zhou, X. He, M. Li, Roles of doping in enhancing the performance of graphene/graphene-like semiconductors, AIP Adv 15 (2025) 010701, https://doi.org/10.1063/5.0248505.

[37] E. Koo, S.-Y. Ju, Role of residual polymer on chemical vapor grown graphene by Raman spectroscopy, Carbon 86 (2015) 318–324, https://doi.org/10.1016/j.carbon.2015.01.055.

[38] H. Raza, Graphene Nanoelectronics: Metrology, Synthesis, Properties and Applications, Springer, Berlin Heidelberg, Berlin, Heidelberg, 2012, https://doi.org/10.1007/978-3-642-22984-8.

[39] S.J. Kim, S.J. Park, H.Y. Kim, G.S. Jang, D.J. Park, J.-Y. Park, S. Lee, Y.H. Ahn, Characterization of chemical doping of graphene by *in-situ* raman spectroscopy, Appl. Phys. Lett. 108 (2016) 203111, https://doi.org/10.1063/1.4950969.

[40] Z. Hu, Y. Zhao, W. Zou, Q. Lu, J. Liao, F. Li, M. Shang, L. Lin, Z. Liu, Doping of graphene films: open the way to applications in electronics and optoelectronics, Adv. Funct. Mater. 32 (2022) 2203179, https://doi.org/10.1002/adfm.202203179.

[41] D.M. Basko, S. Piscanec, A.C. Ferrari, Electron-electron interactions and doping dependence of the two-phonon raman intensity in graphene, Phys. Rev. B 80 (2009) 165413, https://doi.org/10.1103/PhysRevB.80.165413.

[42] N.S. Mueller, S. Heeg, M.P. Alvarez, P. Kusch, S. Wasserroth, N. Clark, F. Schedin, J. Parthenios, K. Papagelis, C. Galiotis, M. Kalbáč, A. Vijayaraghavan, U. Huebner, R. Gorbachev, O. Frank, S. Reich, Evaluating arbitrary strain configurations and doping in graphene with Raman spectroscopy, 2D Mater 5 (2017) 015016, https://doi.org/10.1088/2053-1583/aa90b3.

[43] J.E. Lee, G. Ahn, J. Shim, Y.S. Lee, S. Ryu, Optical separation of mechanical strain from charge doping in graphene, Nat. Commun. 3 (2012) 1024, https://doi.org/10.1038/ncomms2022.

[44] M. Huang, H. Yan, T.F. Heinz, J. Hone, Probing strain-induced electronic structure change in graphene by raman spectroscopy, Nano Lett. 10 (2010) 4074–4079, https://doi.org/10.1021/nl102123c.

[45] J. Tesch, F. Paschke, M. Fonin, M. Wietstruk, S. Böttcher, R.J. Koch, A. Bostwick, C. Jozwiak, E. Rotenberg, A. Makarova, B. Paulus, E. Voloshina, Y. Dedkov, The graphene/n-Ge(110) interface: structure, doping, and electronic properties, Nanoscale 10 (2018) 6088–6098, https://doi.org/10.1039/c8nr00053k.

[46] J. Sitek, I. Pasternak, J. Grzonka, J. Sobieski, J. Judek, P. Dabrowski, M. Zdrojek, W. Strupinski, Impact of germanium substrate orientation on morphological and structural properties of graphene grown by CVD method, Appl. Surf. Sci. 499 (2020) 143913, https://doi.org/10.1016/j.apsusc.2019.143913.

[47] J. Tesch, F. Paschke, M. Fonin, M. Wietstruk, S. Böttcher, R.J. Koch, A. Bostwick, C. Jozwiak, E. Rotenberg, A. Makarova, B. Paulus, E. Voloshina, Y. Dedkov, The graphene/n-Ge(110) interface: structure, doping, and electronic properties, Nanoscale 10 (2018) 6088–6098, https://doi.org/10.1039/C8NR00053K.

[48] I.Yu. Evchuk, R.I. Musii, R.G. Makitra, R.E. Pristanskii, Solubility of polymethyl methacrylate in organic solvents, Russ. J. Appl. Chem. 78 (2005) 1576–1580, https://doi.org/10.1007/s11167-005-0564-9.

[49] R. Wang, R. Yang, Z. Ren, B. Zhang, Q. Lu, M. Yi, Y. Luo, Quantitative relationship between surface chemistry of graphene and compatibility with rubbers established by two-dimensional solubility parameters, RSC Adv 14 (2024) 39081–39093, https://doi.org/10.1039/D4RA08062A.

[50] C. Neumann, S. Reichardt, P. Venezuela, M. Drögeler, L. Banszerus, M. Schmitz, K. Watanabe, T. Taniguchi, F. Mauri, B. Beschoten, S.V. Rotkin, C. Stampfer, Raman spectroscopy as probe of nanometre-scale strain variations in graphene, Nat. Commun. 6 (2015) 8429, https://doi.org/10.1038/ncomms9429.

[51] N.J.G. Couto, D. Costanzo, S. Engels, D.-K. Ki, K. Watanabe, T. Taniguchi, C. Stampfer, F. Guinea, A.F. Morpurgo, Random strain fluctuations as dominant disorder source for high-quality on-substrate graphene devices, Phys. Rev. X 4 (2014) 041019, https://doi.org/10.1103/PhysRevX.4.041019.

[52] A.R. Flanagan, F.G. Glavin, Open-source Raman spectra of chemical compounds for active pharmaceutical ingredient development, Sci. Data 12 (2025) 498, https://doi.org/10.1038/s41597-025-04848-6.